Journal of Power Sources 262 (2014) 178–182

Contents lists available at ScienceDirect

Journal of Power Sources

journal homepage: www.elsevier.com/locate/jpowsour

Short communication

Size-dependent capacitance of NiO nanoparticles synthesized with cathodic contact glow discharge electrolysis

Anis Allagui [a,*], Abdul Hai Alami [a], Elena A. Baranova [b], Rolf Wüthrich [c,*]

[a] Sustainable and Renewable Energy Engineering, University of Sharjah, PO Box 27272, Sharjah, United Arab Emirates
[b] Department of Chemical and Biological Engineering, University of Ottawa, 161 Louis-Pasteur, Ottawa, ON K1N 6N5, Canada
[c] Department of Mechanical and Industrial Engineering, Concordia University, 1455 de Maisonneuve Blvd. West, Montreal, QC H3G 1M8, Canada

HIGHLIGHTS

- Synthesis of NiO nanoparticles by CGDE for electrochemical energy storage.
- Capacitance of NiO nanoparticles is size-dependent.
- 218 F g^{-1} for 70 nm NiO nanoparticles, @2.7 A g^{-1} in 1 M KOH.

ARTICLE INFO

Article history:
Received 11 November 2013
Received in revised form
11 February 2014
Accepted 22 March 2014
Available online 29 March 2014

Keywords:
Pseudocapacitance
Nickel oxide
Glow discharge electrolysis
Plasma micro-discharges

ABSTRACT

NiO nanoparticles of 70, 91 and 107 nm average diameter are synthesized by cathodic contact glow discharge electrolysis at 30, 36 and 42 VDC respectively, in 2 M H_2SO_4 + 0.5 M ethanol + 2.5 mg ml^{-1} of PVP, and are investigated for electrochemical energy storage. From the cyclic voltammetry and galvanostatic charge–discharge measurements in 1 M KOH, it was found that a maximum specific capacitance of 218 F g^{-1} is achieved with the 70 nm NiO nanoparticles at 2.7 A g^{-1}. Larger nanoparticles of 91 and 107 nm diameter exhibit specific capacitances of 106 and 63 F g^{-1}, respectively, suggesting a size-dependent capacitive performance enhanced with decreasing particles size.

1. Introduction

The continuous increase of consumption and demand for the ecologically non-friendly fossil fuel has pushed more and more towards the development of other sustainable sources of energy. Electric energy generated from solar radiation and wind turbines is not continuous in time and thus there is a need to implement reliable energy storage systems along with these power production processes [1]. Additionally, the ongoing miniaturization of power sources for the fast expanding market of portable devices is in need for advanced energy storage solutions. Electrochemical energy storage technologies of electric double-layer capacitors are already on the market but they are restricted to the non-faradic processes of high surface area carbon-based materials, while conductive polymers, although having promising capacitive performance, can be expensive and involve complex multi-step synthesis processes [2–5]. Supercapacitors, on the other hand, exhibit higher degree of reversibility (longer cycle life) and higher power density when compared to batteries, and higher energy density when compared to electric double-layer capacitors [6,7]. Supercapacitors are the subject of intense research activity for energy storage applications, and can be classified into two types depending on their charge-storage mechanism [8–11]:

- the electric double-layer capacitor, which is based on the capacitance due to the very small distance between the charges on the electrode surface and their opposite charges provided by the electrolyte, and
- the pseudocapacitor, which is based on the charge transfer generated by the quasi-reversible faradic reactions at the electrode surface, and formed during the anodic polarization. The origin of the capacitance in this case is faradic, not electrostatic.

The capacitance of a supercapacitor is therefore the sum of the double-layer capacitance with the pseudocapacitance due to the redox reaction: $Ox_{ad} + ze^- \rightarrow Red_{ad}$ [8,11].

* Corresponding authors.
E-mail addresses: aallagui@sharjah.ac.ae (A. Allagui), rolf.wuthrich@concordia.ca (R. Wüthrich).

http://dx.doi.org/10.1016/j.jpowsour.2014.03.104
0378-7753/

Ideal electrode materials for supercapacitors based on ruthenium oxides are known for their high mass-specific capacitances that can reach several hundreds of farads per gram. For example, Kim et al. reported 620 F g^{-1} for composites of carbon nanotube with RuO_2 nanoparticles synthesized by microwave-polyol [12], while Zheng et al. reported values as high as 720 F g^{-1} for the amorphous hydrous ruthenium oxide ($RuO_2 \cdot xH_2O$) material prepared by the sol–gel technique [13]. Due to the rarity, toxicity and high cost of this noble metal, alternative solutions using oxides of more abundant and inexpensive transition metals such as nickel, cobalt and manganese are under extensive investigation [1,11,8–10,14–20]. Table 1 gives some recently reported examples of electrode materials, as well as their working conditions and specific capacitances values. NiO and $Ni(OH)_2$ are indeed viewed as promising electrode materials for energy storage applications due to their i) excellent electrochemical performance with high theoretical specific capacitance, ii) abundance and low cost, as well as their iii) good capacitive retention and stability in corrosive alkaline conditions [18,10]. In addition, at the nano-scale, nickel oxides/hydroxides are expected to exhibit superior properties when compared to their bulk counterpart, as less material is necessary and much higher surface area can be achieved.

The physicochemical properties of nanoparticles depend, amongst others, on the synthesis method and on the size and shape of the particles. Nickel oxides have been prepared with various techniques, such as the hydrothermal method [21], chemical precipitation [22] and chemical spray pyrolysis [23], to cite a few. It is worth mentioning that the literature on the size-dependency of capacitive capabilities of nickel-based nanomaterials is very scarce to date. In this paper we report the electrochemical energy storage performance of three sizes of NiO nanomaterials, namely 70, 91 and 107 nm, synthesized by cathodic contact glow discharge electrolysis (CGDE) [24]. Mass-specific capacitances and energy and power densities of the investigated particles are evaluated by cyclic voltammetry and constant current charge–discharge measurements.

2. Experimental

The synthesis of nickel oxide nanoparticles by cathodic CGDE along with the characterization of their morphology and crystal structure are detailed in a previous publication [24]. It consists of two electrodes of nickel, immersed in a solution of 2 M H_2SO_4 + 0.5 M ethanol + 2.5 mg ml^{-1} of PVP40, and subject to three different constant terminal voltages using a TDK Lambda 60 V–3.5 A DC power supply. Different from low-current electrochemistry, when the terminal voltage in a two-electrode cell is set higher than a critical value ($\approx$18 VDC for the present solution of 2 M H_2SO_4 + 0.5 M ethanol + 2.5 mg ml^{-1} of PVP40, using a Ni wire cathode vs. a much larger Ni anode [24]), one can observe the transition from the conventional electrolysis to the emission of visible light from the active electrode. At the three terminal voltages 30, 36 and 42 VDC, current flows through a dielectric gaseous envelope formed around the active electrode as glow micro-discharges. The intermittent electrical discharges are the source of remarkable non-Faradaic chemical yields and free radical species able to reduce the Ni ions provided by the Ni anode dissolution to form nanoparticles of Ni-based materials. In acidic media, pure NiO phase was obtained, while in alkaline pH, β-$Ni(OH)_2$ was the main product due to the electro-erosion of the micro-plasma-covered electrode [24–26].

Mean values and variances of the samples size distribution of NiO nanoparticles were estimated from electron micrographs image processing obtained by a JEOL JSM-7500F FESEM. We found the sample variables ($\bar{x}$ = 91 nm; s^2 = 97 nm^2), ($\bar{x}$ = 70 nm; s^2 = 49 nm^2) and ($\bar{x}$ = 107 nm; s^2 = 53 nm^2) for the particles synthesized at 30, 36 and 42 VDC respectively [24]. Powder X-ray diffraction (XRD) patterns of the as-synthesized particles were acquired with a Philips X'Pert Pro Multipurpose X-ray diffractometer (Cu K_α source, λ = 1.5404 Å) at 40 kV–45 mA, in the 2θ range 30–85° with 0.02° 2θ s^{-1} scanning rate. Fig. 1 shows both a typical electron micrograph and XRD patterns of NiO nanoparticles synthesized at 36 VDC with cathodic CGDE in acidic medium. The typical crystal planes (111), (200), (220), (311) and (222) of fcc NiO (bunsenite, NaCl type structure), perfectly indexed with PDF-4+ (ICDD) 04-011-8441 data file [24] are shown in Fig. 1(b). Absence of any secondary peaks shows the stoichiometric purity of the NiO products.

The preparation of electrodes for the electrochemical measurements is done by depositing 20 µl from a sonicated nanoparticles-in-ethanol solution onto the cross-section of a 5 mm

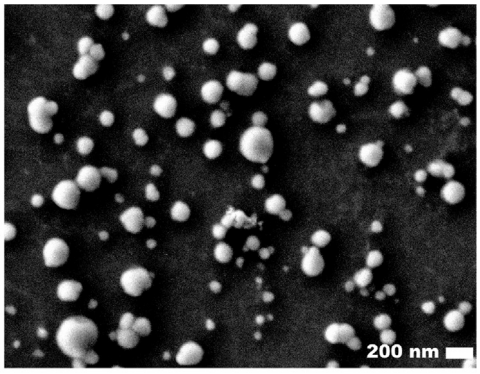

(a)

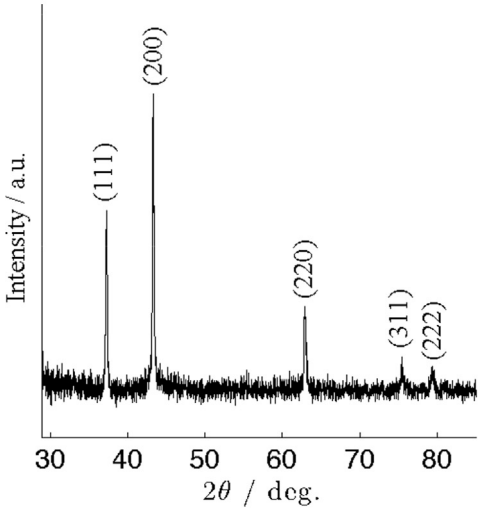

(b)

Fig. 1. SEM micrograph (a) and powder XRD patterns (b) of NiO nanoparticles (⌀ = 70 nm) synthesized by cathodic CGDE with Ni cathode vs. Ni anode in 2 M H_2SO_4 + 0.5 M EtOH + 2.5 mg ml^{-1} of PVP at 36 VDC.

Table 1
Specific capacitance of selected electrode materials.

Materials	Working conditions	c_{sc}/F g^{-1}
NiO nanoparticles [18]	−0.2 to 0.6 V in 1 M KOH	370 at 2 A g^{-1}
NiO_x xerogels [19]	0.2–0.6 V in 7 M KOH	696 at 2 mA cm^{-2}
β-$Ni(OH)_2$ nanoparticles [10]	0–0.55 V in 1 M KOH	715 at 0.5 A g^{-1}
$Ni(OH)_2$ film [9]	0–0.55 V in 0.5 M KOH	578 at 0.5 A g^{-1}
MnO_2 [36]	0–0.8 V in 0.1 M Na_2SO_4	318 at 2.3 A g^{-1}
Co_3O_4 aerogels [20]	−0.1 to 0.55 V 1 M NaOH	623 at 25 mV s^{-1}

diameter graphite rod freshly polished and washed with deionized water. The material loading is estimated to *ca.* 0.5 mg cm^{-2}. The working electrode is then left to dry for 5 min in oven preset at 70 C. All of the potentiodynamic and galvanostatic charge-discharge experiments are conducted at room temperature with an Amel Electrochemistry potentiostat model 7050 in a multi-neck round-bottom flask, with a Pt wire serving as a counter electrode and Ag/AgCl/KCl (saturated) as reference electrode. The supporting electrolyte for all measurements is KOH at unit molarity.

3. Results and discussion

3.1. Cyclic voltammetry

The cyclic voltammograms of the prepared electrodes are performed in the potential range 0–0.6 V vs. Ag/AgCl in 1 M KOH at the scan rates 5, 10, 20, 30 and 50 mV s^{-1}. Fig. 2 illustrates the set of voltammograms of NiO nanoparticles prepared by cathodic CGDE at 36 V ($\varnothing = 70$ nm). The potentiodynamic features of the two other electrode materials ($\varnothing = 91$ and 107 nm, not shown here) exhibit similar trends. Their capacitive performance will be detailed and compared in Section 3.3. The voltammograms in Fig. 2 represent the last cycle in a series of potential sweeps where the electrochemical responses of the electrode were stable and did not significantly change from one cycle to another. The stabilization of the electrode behavior is usually achieved after 8–10 cycles. The *y*-axis shows the current density per unit mass of the synthesized products weighed with a microgram-precision balance. The voltammograms are different from the rectangular ones, and maintain their shapes with the variation of scan rates, which is typical for pseudocapacitive behavior [18,27,21]. However, there is a slight positive shift of the anodic peak with the increase of the scan rate which indicates some kinetic irreversibility in the electrochemical system [7,28]. This can also be deducted from the asymmetry of the positive vs. negative sweeps in the voltammograms. In the alkaline solution used, the following surface faradic charge-discharge reactions occur [18,21,29–31]:

$$\mathrm{NiO} + z\mathrm{OH}^- \underset{\text{discharge}}{\overset{\text{charge}}{\rightleftharpoons}} z\mathrm{NiOOH} + (1-z)\mathrm{NiO} + ze^- \qquad (1)$$

where $0 < z < 1$ is the fraction of available sites at NiO materials for the reaction with OH^- ions. The peaks corresponding to the redox reactions Ni(II)/Ni(III) are centered at *ca.* 0.50 V and 0.39 V vs Ag/AgCl, respectively. The onset of the oxygen evolution reaction takes place at *ca.* 0.55 V. The quasi-perfect linearity of the anodic peak current density versus the square root of the scan rate, illustrated in the insert of Fig. 2, confirms that the redox reactions are diffusion-limited (from Randle–Sevcik equation), as well as their contribution in the pseudocapacitive behavior of the electrode materials [32,18,33,9].

The average capacitance per unit mass, c_{sc}, is estimated from the cyclic voltammograms by graphically integrating the total charge over the voltage range according to [10,31,18,5]:

$$c_{sc} = \frac{1}{m s_r (V_a - V_c)} \int_{V_a}^{V_c} I dV \qquad (2)$$

where m is the mass of deposited NiO nanoparticles, s_r the voltage scan rate, $V_a - V_c = \Delta V$ the potential window 0–0.55 V, and $I(V)$ the total current. The specific current densities of the anodic peaks in Fig. 2 are 12.7, 9.1, 7.0, 4.4 and 2.7 A g^{-1} for the scan rates of 50, 30, 20, 10, and 5 mV s^{-1}, respectively, to which correspond the calculated specific capacitance values of 122, 135, 156, 170 and 200 F g^{-1}. The inverse variation of c_{sc} with the scan rate is due to the smaller fractions of OH^- ions reaching the electro-active NiO sites, as the system is diffusion-limited. On the contrary, with low voltammetric scan rates, higher fractions of OH^- involved in Reaction (1) will have more favorable conditions to access the NiO nanoparticles, and thus leading to higher available capacitance [34]. These observations are also found for the 91 and 107 nm NiO nanomaterials.

3.2. Chronopotentiometry

Galvanostatic charge-discharge curves at the different constant current densities 12.7, 7.0, 4.4 and 2.7 A g^{-1} (see Fig. 2), within the potential range 0–0.50 V vs. Ag/AgCl of the NiO nanoparticles synthesized at 36 VDC are illustrated in Fig. 3. Independently of the applied current density, the charging step in Fig. 3 shows two stages: the first linear one corresponds to the oxidation of NiO, whereas the second one corresponds to the charging process itself. On the other hand, the discharging curve shows first a sharp negatively-sloped segment of potential drop due to the internal resistance followed by a slowly decaying second part, related to the pseudocapacitive behavior of the electrode material.

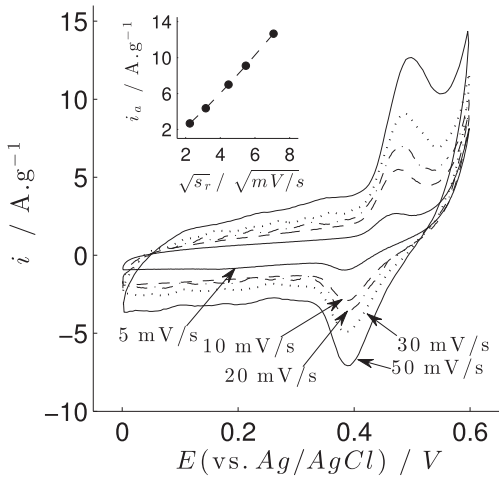

Fig. 2. Cyclic voltammograms and evolution of anodic peak current density with the square root of the scan rate (insert) of NiO nanoparticles ($\varnothing = 70$ nm).

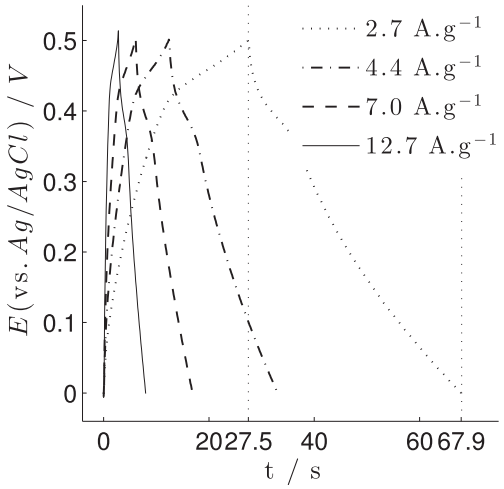

Fig. 3. Constant current charge–discharge response of NiO nanoparticles ($\varnothing = 70$ nm) at 12.7, 7.0, 4.4 and 2.7 A g^{-1}.

The average specific capacitance, assumed to be invariant with the potential, is calculated from the discharge curves as follows.

$$c_{sc} = \frac{I\Delta t}{m\Delta V} \quad (3)$$

where I is the applied current, Δt the discharge time, m the mass of deposited NiO nanoparticles and ΔV the potential window. For example, at the current density 2.7 A g^{-1}, the mass-specific capacitance is $2.7 \times (67.9 - 27.5)/0.5 = 218$ F g^{-1}. At the current densities 12.7, 9.1, 7.0 and 4.4 A g^{-1}, the specific capacitances from the charge–discharges curves are found to be 131, 143, 169 and 182 F g^{-1} respectively. Again, because of the diffusion-controlled redox reaction between the OH^- ions and the NiO nanoparticles, the specific capacitance increases for lower charge-discharge rates. The values of c_{sc} are in line with the ones estimated from the cyclic voltammetry measurements.

3.3. Ragone plots

Two important parameters measuring the performance of a capacitive device, that is, the specific energy density, d_e, and specific power, d_p, are well represented with Ragone plots. The energy density of the NiO materials synthesized at 36 VDC ($\varnothing = 70$ nm), calculated as $d_e = c_{sc}(\Delta V)^2/2$, and the power density calculated as $d_p = d_e/\Delta t$ from the chronopotentiometric results, are plotted in Fig. 4 with respect to the applied current density.

The performance characteristics of the NiO nanomaterials synthesized by cathodic CGDE are clearly that of a supercapacitor, with energy densities varying from almost 100 to 54 Wh kg^{-1} at current densities varying from 2.7 to 12.7 A g^{-1} in the narrow potential window of 0–0.50 V vs. Ag/AgCl. Coupling the NiO nanomaterials with a suitable counter electrode in order to achieve higher energy and power density values over a wider operating voltage is the next step for this study.

Following the same procedure for the calculation of the specific capacitances from the charge–discharge plots, the power and energy performance of NiO nanoparticles, prepared by cathodic CGDE at 30 ($\varnothing = 91$ nm), 36 ($\varnothing = 70$ nm) and 42 VDC ($\varnothing = 107$ nm) are compared. Ragone plots of the analyzed NiO nanomaterials are shown in Fig. 5. It is clear that the particles of 70 nm average diameter exhibit the highest energy and power densities when compared to the larger ones (91 nm and 107 nm), and thus are more suitable for energy storage applications. Additionally, the samples synthesized at 42 VDC were found to be severely sintered

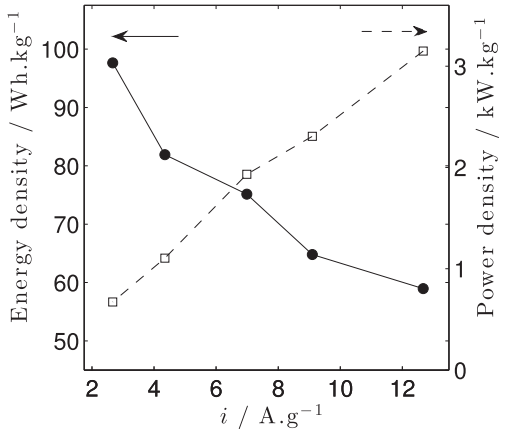

Fig. 4. Energy and power densities vs. current density of NiO nanoparticles ($\varnothing = 70$ nm).

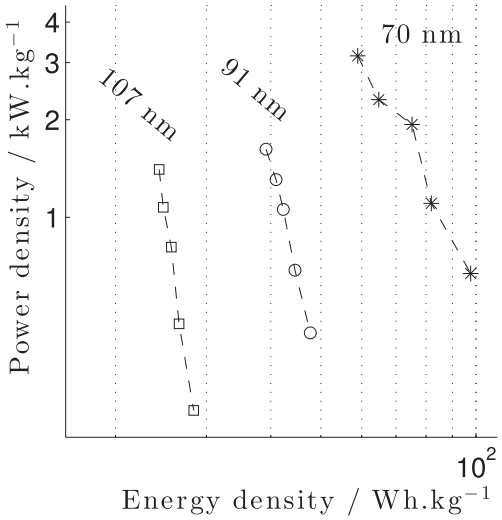

Fig. 5. Ragone plots of 70, 91 and 107 nm average diameter NiO nanoparticles. The electric values are derived from the respective constant current charge–discharge measurements.

and agglomerated when compared to the two other samples, due to the high local discharge activity and temperature at these electric conditions [24]. The OH^- ions involved in the redox reaction (1) have better accessibility to the NiO nanoparticles of smaller size and less agglomeration, due to their larger active surface area, compared to larger particles. Pico et al. reported the same trend of the size effect on the specific capacitance of RuO_2 in the sub-5 nm range [35].

4. Conclusion

Three sizes of NiO nanoparticles, namely, 70, 91 and 107 nm, prepared by cathodic CGDE in acidic medium, were tested for electrochemical energy storage applications. It is found that the smaller and the more dispersed the particles are, the higher the specific capacitance will be, since the pseudocapacitance is based on faradic charge-transfer reactions with the OH^- ions and is dependent on its accessibility to the NiO materials. For example, NiO nanoparticles manufactured at 36 VDC by cathodic CGDE and with an average size of 70 nm are able to store charges with a specific capacitance as high as 218 F g^{-1} at 2.7 A g^{-1}. Their corresponding energy and power densities are 98.1 Wh kg^{-1} and 0.7 kW kg^{-1}, respectively. On the other hand, NiO manufactured at 30 VDC with average size of 91 nm have a specific capacitance of 106 F g^{-1} at 1.76 A g^{-1}, with $d_e = 47.7$ Wh kg^{-1} and $d_p = 0.44$ kW kg^{-1}. Larger and agglomerated particles manufactured at 42 VDC ($\varnothing = 107$ nm) still exhibit pseudocapacitance behavior with $c_{sc} = 63$ F g^{-1} at 1 A g^{-1}, $d_e = 28.4$ Wh kg^{-1} and $d_p = 0.25$ kW kg^{-1}.

References

[1] Qi Lu, Michael W. Lattanzi, Yunpeng Chen, Xiaoming Kou, Wanfeng Li, Xin Fan, Karl M. Unruh, Jingguang G. Chen, John Q. Xiao, Angew. Chem. Int. Ed. 123 (30) (2011) 6979–6982.
[2] E. Gomibuchi, T. Ichikawa, K. Kimura, S. Isobe, K. Nabeta, H. Fujii, Carbon 44 (5) (2006) 983–988.
[3] L. Wei, G. Yushin, J. Power Sources 196 (8) (2011) 4072–4079.
[4] A. Balducci, W.A. Henderson, M. Mastragostino, S. Passerini, P. Simon, F. Soavi, Electrochim. Acta 50 (11) (2005) 2233–2237.
[5] J.-H. Kim, Y.-S. Lee, A.K. Sharma, C.G. Liu, Electrochim. Acta 52 (4) (2006) 1727–1732.
[6] B.E. Conway, E. Gileadi, Trans. Faraday Soc. 58 (1962) 2493–2509.
[7] B.E. Conway, J. Electrochem. Soc. 138 (6) (1991) 1539–1548.

[8] Y. Zhang, H. Feng, X. Wu, L. Wang, A. Zhang, T. Xia, H. Dong, X. Li, L. Zhang, Int. J. Hydrogen Energy 34 (11) (2009) 4889–4899.
[9] D.-D. Zhao, S.-J. Bao, W.-J. Zhou, H.-L. Li, Electrochem. Commun. 9 (5) (2007) 869–874.
[10] M. Aghazadeh, A.N. Golikand, M. Ghaemi, Int. J. Hydrogen Energy 36 (14) (2011) 8674–8679.
[11] A. Shukla, S. Sampath, K. Vijayamohanan, Curr. Sci. 79 (12) (2000) 1656–1661.
[12] J.-Y. Kim, K.-H. Kim, S.-H. Park, K.-B. Kim, Electrochim. Acta 55 (27) (2010) 8056–8061.
[13] J.P. Zheng, P.J. Cygan, T.R. Jow, J. Electrochem. Soc. 142 (8) (1995) 2699–2703.
[14] S.-C. Pang, M.A. Anderson, T.W. Chapman, J. Electrochem. Soc. 147 (2) (2000) 444–450.
[15] F. Tao, C. Gao, Z. Wen, Q. Wang, J. Li, Z. Xu, J. Solid State Chem. 182 (5) (2009) 1055–1060.
[16] C. Lin, J.A. Ritter, B.N. Popov, J. Electrochem. Soc. 145 (12) (1998) 4097–4103.
[17] C. Lokhande, D. Dubal, O.-S. Joo, Curr. Appl. Phys. 11 (3) (2011) 255–270.
[18] S.K. Meher, P. Justin, G. Ranga Rao, ACS Appl. Mater. Interfaces 3 (6) (2011) 2063–2073.
[19] J. Cheng, G.-P. Cao, Y.-S. Yang, J. Power Sources 159 (1) (2006) 734–741.
[20] T.-Y. Wei, C.-H. Chen, K.-H. Chang, S.-Y. Lu, C.-C. Hu, Chem. Mater. 21 (14) (2009) 3228–3233.
[21] Y.-Z. Zheng, H.-Y. Ding, M.-L. Zhang, Mater. Res. Bull. 44 (2) (2009) 403–407.
[22] Y. Zheng, M. Zhang, P. Gao, Mater. Res. Bull. 42 (9) (2007) 1740–1747.
[23] L. Cattin, B. Reguig, A. Khelil, M. Morsli, K. Benchouk, J. Bernède, Appl. Surf. Sci. 254 (18) (2008) 5814–5821.
[24] A. Allagui, R. Wüthrich, Electrochim. Acta 58 (2011) 12–18.
[25] A. Allagui, E.A. Baranova, R. Wüthrich, Electrochim. Acta 93 (2013) 137–142.
[26] R. Wüthrich, A. Allagui, Electrochim. Acta 55 (27) (2010) 8189–8196.
[27] J. Chang, M. Park, D. Ham, S. Ogale, R.S. Mane, S.-H. Han, Electrochim. Acta 53 (15) (2008) 5016–5021.
[28] S.K. Meher, P. Justin, G.R. Rao, Electrochim. Acta 55 (28) (2010) 8388–8396.
[29] W. Xing, F. Li, Z. feng Yan, G.Q. Lu, J. Power Sources 134 (2) (2004) 324–330.
[30] V. Srinivasan, J.W. Weidner, J. Electrochem. Soc. 147 (3) (2000) 880–885.
[31] V. Srinivasan, J.W. Weidner, J. Power Sources 108 (1–2) (2002) 15–20.
[32] G.R. Fu, Z.A. Hu, L.J. Xie, X.Q. Jin, Y.L. Xie, Y.X. Wang, Z.Y. Zhang, Y.Y. Yang, H.Y. Wu, Int. J. Electrochem. Sci. 4 (2009) 1052–1062.
[33] Y. Gang Wang, Y. Yao Xia, Electrochim. Acta 51 (16) (2006) 3223–3227.
[34] W. Pell, B. Conway, J. Electroanal. Chem. 500 (1–2) (2001) 121–133.
[35] F. Pico, J. Ibaņez, M. Lillo-Rodenas, A. Linares-Solano, R. Rojas, J. Amarilla, J. Rojo, J. Power Sources 176 (1) (2008) 417–425.
[36] J. Liu, J. Essner, J. Li, Chem. Mater. 22 (17) (2010) 5022–5030.